5. MONTE CARLO SIMULATIONS OF NaI(TL) SCINTILLATION DETECTORS FOR MULTI-PHASE FLOW MAPPING AND VISUALIZATION USING CARPT

A Monte Carlo based simulation strategy has been developed for determining the total and photopeak efficiencies of cylindrical NaI(Tl) scintillation detectors for an arbitrarily located point γ-ray source in the three-dimensional space. Improved computational efficiency, in evaluating the intrinsic photopeak efficiency of the detectors, has been achieved by using Gaussian quadratures for carrying out multi-dimensional integration, instead of the frequently used uniform sampling in conventional Monte Carlo methods. It is observed that the photopeak efficiency is not a constant, and varies with the position of the γ-ray point source. A generalized reduced gradient optimization scheme has been applied to optimize for the detector gains and dead-times, which are needed for the construction of a detailed 3-D calibration map to dynamically locate the position of the radioactive particle. An efficient computational scheme has also been developed to compute the particle position from the dynamic count data. This scheme uses a chi-square minimization in conjunction with 3-D interpolation to provide improved accuracy in locating the particle position.

5.1. Introduction

The Computer Automated Radioactive Particle Tracking (CARPT) has been proven to be an excellent tool for studying the flow pattern/mixing mechanisms in multiphase reactors (Devanathan, 1991; Devanathan *et al*., 1990, Dudukovic *et al*., 1997). Improvements and changes in the CARPT facility are made from time to time to make it suitable to study various reactor systems. One issue that has always been a bottleneck in the use of CARPT, is the need for an in-situ calibration procedure. Traditional implementation of the technique requires a tedious and time-consuming calibration at each operating condition in the reactor geometry under investigation. During calibration for a given operating condition, the current procedure requires the construction of a **distance-count** map for each detector, by placing a radioactive particle, the flow follower, in a few hundred to a thousand or more known locations over the entire reactor volume. This is currently achieved by mounting the radioactive particle on fishing lines, fixed between two grids at the two ends of the reactor, and manually moving the particle to various locations in the column. All the calibration data are taken at the operating conditions of interest in order for the distance-count maps to properly reflect the hold-up variations. Once the entire calibration map is available for each detector, the dynamic position of this tracer particle can be computed from the instantaneous counts data acquired by the detectors. Time-differentiation of the instantaneous position data provides the instantaneous velocity of the particle. The application of the ergodic hypothesis to the ensemble-averaged data results in the evaluation of the time-averaged velocity and turbulence-parameter fields over the entire reactor volume.

The Monte Carlo simulation of detector photopeak efficiencies offers an alternative to this tedious in-situ calibration procedure. It is based on an approach where the radioactive-

count received by a detector is modeled, as opposed to a heuristically based current procedure. When a radioactive particle is used as a phase follower in multiphase flows, the intervening medium between the point source and the detector consists of the reactor media and the reactor wall (as well as insulation if present). Thus, appropriate geometrical arguments have to be used to compute the probability of non-interaction of the γ-ray photon with the media in between the radioactive source and the detector. Additionally, the technique has the advantage of determining the dynamic location of the radioactive particle from the counts registered by all the detectors, using previously constructed (obtained by using the Monte Carlo simulations) 3-D position-counts map for each detector. This improves the accuracy of locating the particle position from count data received by each detector, since 3-D mapping is being used instead of 1-D mapping from in-situ calibration.

5.2. Research Objectives

The literature on the application of Monte Carlo technique for simulating the photo-peak efficiency of a cylindrical NaI(Tl) detector in response to a single point source has been well studied. It is the aim of this work to extend this firm theoretical basis by applying it to more complex geometries and media configurations, as present in a reactor with multi-phase flow. Specifically, the objectives are:

1) Develop Monte Carlo programs to calculate the intrinsic efficiency of a cylindrical NaI(Tl) detector due to a point source located at any position inside the reactor volume.
2) Validate these programs by comparing the simulation results from this work with the available Monte Carlo simulation as well as experimental data for a point source located on the axis of a cylindrical detector.
3) Verify the simulation results by comparing the simulated counts to those measured at a number of known locations inside a reactor. Optimize detector dead-time constants, detector gains and the linear attenuation coefficient of the reactor media (function of the local media density) to best match the experimental and theoretical data.
4) Develop programs to generate 3-D position-count calibration maps for each detector using the optimized variables obtained above for each detector.
5) Generate source codes to dynamically determine the particle position by inverse mapping the counts from each detector against the position-count map obtained from Monte Carlo simulations above.
6) Verify the accuracy of the inverse-mapping programs by comparing the predicted particle position with its actual position by placing the radioactive particle into several known locations.
7) Integrate all the programs developed above to process data from actual CARPT experiments.

5.3. Mathematical Description

The basic framework for implementation of this technique has been provided by Beam *et al*. (1978). They discuss the application of Monte Carlo simulation for the calculation of efficiencies of right-circular cylindrical NaI detectors for arbitrarily located γ-ray emitting radioactive point sources. They successfully show that Monte Carlo calculations can provide NaI detector efficiencies at any specified energy, without resorting to tedious experimental measurements. In this work, the framework established by Beam *et al.* has been modified to include the presence of the reactor walls, and the two or three phase mixture in the reactor. A similar implementation of the Monte Carlo approach has been demonstrated to be successful by Larachi *et al*. (1994).

The development of Beam *et al.* (1978) does not include the effects due to the cladding material encasing the scintillation crystal or the photo-multiplier mounting. At this moment, these effects are not included in this work either, but some researchers have shown that these effects may be significant, especially when simulating the entire energy spectrum (Nardi, 1970; Steyn *et al.*, 1973; Saito and Moriuchi, 1981). On the other hand, if one is interested in simulating only the photo-peak portion of the energy spectrum, the results appear to be insensitive to the inclusion or non-inclusion of the effects of the cladding material in the simulations. Therefore, the non-inclusion of these effects could be justified for the moment. However, efforts are underway to modify the existing codes to include the presence of the cladding material in order to quantitatively analyze the effect of the cladding material. Also, Beam's analysis considers only Compton and photoelectric interactions, while the production of secondary electrons is neglected. This implies that the photon energies should be less than 1 MeV. This is true of the radioactive particles being used for CARPT (Sc^{46}) and therefore, presents no limitation. In what follows, a brief description of the theoretical basis for this work is discussed.

The Monte Carlo treatment consists of following and categorizing a large number of photon histories from emission at the source to absorption within the detector. **Random number** and **probability theory**, combined with known transport distributions are used to locate the photon collision site, as well as trajectory, energy and direction through each history. As developed by Beam *et al.* (1978), three variance reduction steps are employed during each history:

- Each γ-ray is forced to strike the detector.
- Each γ -ray is forced to interact within the bounds of the detector; i.e., photons are not allowed to escape from the detector.
- Each interaction is forced to be a Compton Scattering event.

A photon history is terminated when either the weight of a scattering interaction (ratio of scattering to total cross-section) or the energy of the photon falls below a specified minimum (e.g. 10^{-10} or 0.01 MeV). Any possibility of bias due to these variance reduction techniques is eliminated by calculating the appropriate weights for each of the above forced events using well-defined physical and geometrical principles.

5.3.1. Determination of Solid Angle

The determination of the solid angle at an arbitrary point by a cylindrical detector can be accomplished by a Monte Carlo calculation. Figure 5.1 shows the position of the point source relative to the detector, which is a known basic input.
The two cases that have to be considered are:

- A point source located in such a position so that the γ-ray photons can enter from the top as well as the side (Figure 5.1).
- A point source located in such a position so that the γ-ray photons can enter only from the top (Figure 5.2).

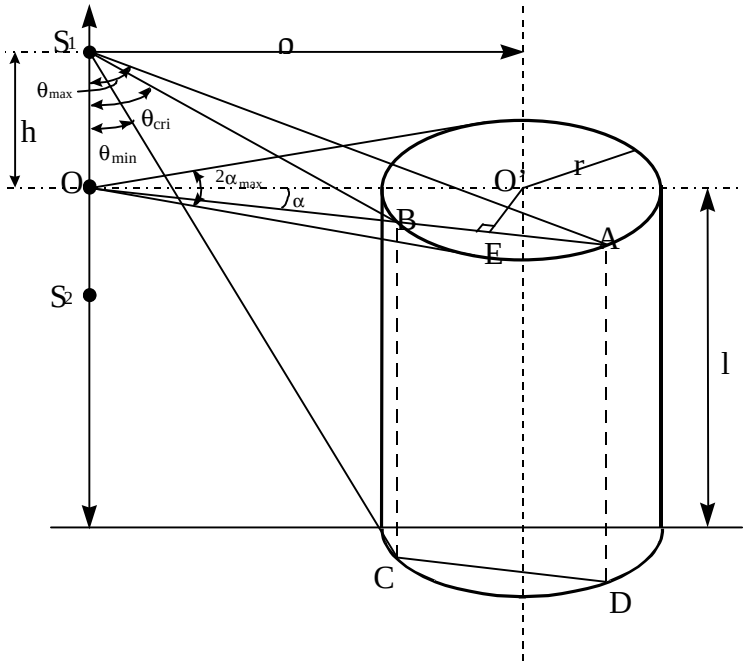

Figure 5.1: Notation Used in the Selection of Angles for Monte Carlo Calculations

From Figure 5.1, we see that if ρ is the distance from the center of the detector to a line parallel to the detector axis, but which contains the point source, and r is the detector radius, then we can define the angle a_{max} as

$$a_{max} = sin^{-1}(r/\rho)$$

The actual angle α is derived from

$$n = \int_{-\alpha_{max}}^{\alpha} \frac{d\alpha}{2\pi} \Big/ \int_{-\alpha_{max}}^{\alpha_{max}} \frac{d\alpha}{2\pi}$$

where, *n* is a random number selected from a uniform distribution between 0 and 1. Consequently,

$$\alpha = \alpha_{max}(2n-1) \qquad -\alpha_{max} \le \alpha \le \alpha_{max}$$

The weighting factor associated with this selection of a, *w (*a), is given by

$$w(\alpha) = \frac{\int_{-\alpha_{max}}^{\alpha_{max}} \frac{d\alpha}{2\pi}}{\int_{0}^{2\pi} \frac{d\alpha}{2\pi}} \qquad w(\alpha) = \frac{\alpha_{max}}{\pi}$$

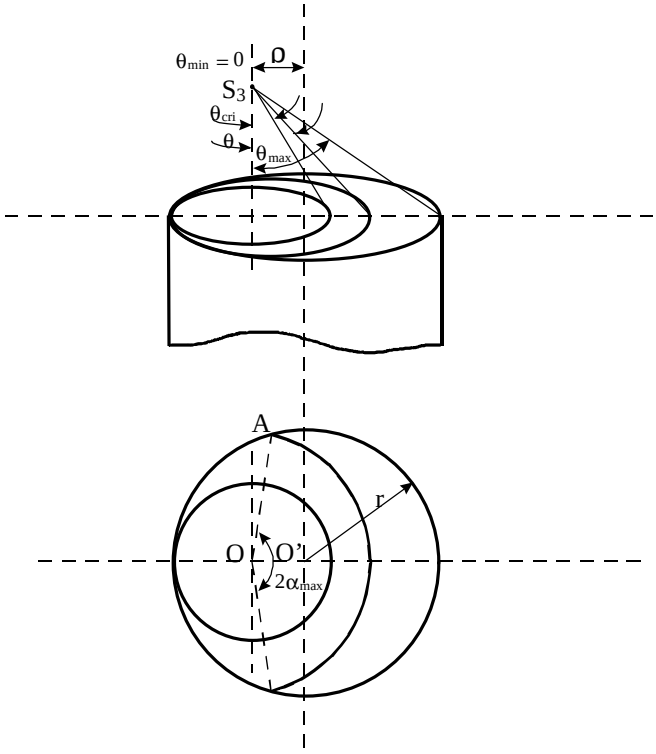

Figure 5.2: Notation for the Case of a Point Source Located Directly Above the Circular Face of the Detector

Once a is randomly selected, the points A, B, C, and D in Figure 5.1 define the plane through which the photon must enter the detector for point sources located at S_1 and S_2 (Beam *et al.*, 1978). Next, one has to define the angles θ_{max} , θ_{cri} *and* θ_{min} to determine the position along the plane through which the photon enters. From Figure 5.1, the line segments *OA* and *OB* can be defined as

$$OA = r\cos a + (r^2 - r^2 \sin^2 a)^{1/2}$$

$$OB = r\cos a - (r^2 - r^2 \sin^2 a)^{1/2}$$

Several cases need to be considered.

Case I When the source is located above the top plane of the detector, for example at S_1 (i.e., when $h \neq 0$)

$\theta_{max} = tan^{-1}(OA/h)$, $\theta_{cri} = tan^{-1}(OB/h)$, $\theta_{min} = tan^{-1}(OB/(h+l))$

Case II When the source is located on the top plane of the detector, for example at O (i.e., when $h = 0$)

$\theta_{max} = \pi/2$, $\theta_{cri} = \pi/2$, $\theta_{min} = \tan^{-1}(OB/l)$

Case III When the source is located below the top plane of the detector, for example at S_2 (i.e., when $h < 0$)

$\theta_{max} = \pi/2 + tan^{-1}(|h|/OB)$, $\theta_{cri} = \pi/2 + tan^{-1}(|h|/OB)$, $\theta_{min} = tan^{-1}(OB/(l-|h|))$

The particular angle θ, which defines the angle along which the photon enters the detector, is chosen using another rectangularly distributed random number n'.

$$n' = \frac{\int_{\theta_{min}}^{\theta} \frac{\sin\theta}{2} d\theta}{\int_{\theta_{min}}^{\theta_{max}} \frac{\sin\theta}{2} d\theta} \qquad \text{or} \qquad \theta = \cos^{-1}\left\{\cos(\theta_{min}) - n'\left[\cos(\theta_{min}) - \cos(\theta_{max})\right]\right\}$$

θ has to be tested to see if the photon enters the top or the side of the detector by comparing it to the angle θ_{cri} defined above. The appropriate weighting factor, $w(\theta)$, for this selection of θ is given by

$$w(\theta) = \frac{\int_{\theta_{min}}^{\theta_{max}} \frac{\sin\theta}{2} d\theta}{\int_{0}^{\pi} \frac{\sin\theta}{2} d\theta} \qquad \text{or} \qquad w(\theta) = \frac{\cos(\theta_{min}) - \cos(\theta_{max})}{2}$$

Case IV When the source is located on top of the detector face, for example at S_3 as in Figure 2

$\theta_{max} = tan^{-1}[(r + \rho)/h]$, $\theta_{cri} = tan^{-1}[(r - \rho)/h]$, $\theta_{min} = 0$

Here, the critical angle, θ_{cri} defines an angle above which the variation of α is limited to $2\alpha_{max}$ and below which angle α may vary over 2π. In the first case, the associated weighting factor, $w(\alpha)$ is the same as defined before, but for the second case, $w(\alpha)$ is

simply equal to 1, as α_{max} is equal to π. Therefore, in this case, θ is calculated first and α is determined knowing the value of θ. Stated mathematically, it translates to

$$\text{For} \quad \theta > \theta_{cri}, \qquad \alpha_{max} = \cos^{-1} \frac{\rho^2 + h^2 \tan^2 \theta - r^2}{2h\rho \tan\theta}$$

$$\text{For} \quad \theta \le \theta_{cri}, \qquad \alpha_{max} = \pi$$

Finally, the total weighting factor for any selection of α and θ in Figures 5.1 and 5.2 is given by

$W_i = w(\theta)\, w(\alpha)$

Where, W_i represents the solid angle subtended for this particular selection of α and θ. The estimate of the solid angle, Ω, is given by the mean value

$$\Omega = \frac{4\pi}{N} \sum_{i=1}^{N} W_i$$

where, N is the total number of histories.

In our implementation of the Monte Carlo method, instead of choosing the photon histories along uniformly distributed (rectangular) random directions as in Beam *et al.* (1978), the angles α and θ are chosen from the Gaussian distributed pseudo-random directions. This reduces the computational demands by around an order of magnitude. If i corresponds to the α–coordinate and j to the θ–coordinate, then

$$x_g(i) = 2n - 1, \qquad x_g(j) = 2n' - 1, \qquad -1 \le x_g(i) \le 1, -1 \le x_g(j) \le 1$$

where, the two random numbers, n and n', are replaced with Gaussian points, $x_g(i)$ and $x_g(j)$ respectively. It has been shown in this work that the results for the photo-peak efficiency are within 1% accuracy with 30 Gaussian points when compared to standard base results computed using 200 Gaussian points.

5.3.2. Photon Interaction with Reactor Media and Detector Crystal

Once the solid angle computation has been accomplished, the next thing to consider is the calculation of the probability of certain type of interaction. We must assess:

a) The probability that γ-rays emitted within Ω would not interact with the reactor media (gas-liquid, gas-liquid-solid mixture) and the reactor wall, f_a

$$f_a(\alpha, \theta) = \exp\left[\sum_{i=1}^{n} \mu_i\, d_i\, (\alpha, \theta)\right]$$

where,

$\mu_i \equiv$ total linear attenuation coefficient of the material i in the γ-ray path.

$d_i \equiv$ distance traveled by the gamma-ray in the direction (α,θ) through reactor media/wall.

$\alpha \equiv$ angle with the line normal to detector axis.

$\theta \equiv$ angle with the detector axis.

b) The probability of interaction (Compton +Photo-Peak) of gamma-rays, emitted within the solid angle, with the detector crystal, f_d

$$f_a(a,q) = 1 - \exp\left[-\mu_d\, d(a,q)\right]$$

where,

$\mu_d \equiv$ total linear attenuation coefficient of the detector crystal.

$d \equiv$ distance traveled through the detector by an undisturbed gamma-ray in the direction (α,θ)

c) The probability of photo-peak interaction of gamma-rays, emitted within the solid angle, with the detector crystal, f_p

$$f_p = w_1 \frac{\tau_1}{\mu_1} + w_\nu \frac{\tau_\nu}{\mu_\nu} \prod_{j=2}^{\nu} w_{j-1} \frac{\sigma_{j-1}}{\mu_{j-1}}$$

$$w_j = 1 - \exp[-\mu_j d_{eff}]$$

where,

$w_1 \equiv$ equal to f_d.

$d_{eff} \equiv$ effective distance traveled by gamma-ray inside the detector.

$\sigma_j \equiv$ attenuation coefficient due to Compton interaction.

$\tau_j \equiv$ attenuation coefficient due to Photo-peak interaction.

$\mu_j = \sigma_j + \tau_j \equiv$ total attenuation coefficient.

$\sigma_j, \tau_j, \mu_j \equiv$ these are all functions of gamma-ray energy, and have to be recomputed after each Compton interaction which changes the gamma-ray (photon)

Having defined f_a, f_d and f_p, the total and photo-peak efficiencies can be calculated by evaluating the following 3_D integrals

$$T_\varepsilon = \iint_\Omega \frac{\vec{r}.\vec{n}}{r^3} f_a(\alpha,\theta) f_d(\alpha,\theta) ds$$

$$P_\varepsilon = \iint_\Omega \frac{\vec{r}.\vec{n}}{r^3} f_a(\alpha,\theta) f_p(\alpha,\theta) ds$$

where,

$\vec{r} \equiv$ vector from the point source to a variable point p on the exposed detector surface.

$n \equiv$ external unit vector locally normal to the surface at point p.

$ds \equiv$ differential area element around point p.

The angles α and θ, as described in Figures 5.1 and 5.2 need to be related to the direction cosines of the γ-ray path from the tracer position to the entry point on the detector surface. This is necessary for determining the distance a γ-ray travels inside the reactor and through the reactor wall. Since the detector axis for all the detectors are perpendicular to the reactor axis, axes rotations and transformations are implemented to make these calculations tractable.

The origin of the initial coordinate system is the center of the reactor bottom plane, z-axis is along the length of the column, and the x-y plane forms the horizontal cross-section of the column. For any particle position (x_p, y_p, z_p inside the reactor) and detector location (x_c, y_c, z_c outside the reactor), the following axis rotations and transformations are performed:

1) Rotation on x-y plane by an angle ω' to make the detector axis parallel to the new x'-axis:

$$\omega' = \tan^{-1}\left(\frac{y_c}{x_c}\right) \qquad x_c > 0$$

$$\omega' = \frac{\pi}{2} \qquad x_c = 0$$

$$\omega' = \pi + \tan^{-1}\left(\frac{y_c}{x_c}\right) \qquad x_c < 0$$

The particle and detector positions in the new coordinate system are x'_p, y'_p and x'_c, y'_c, respectively (z position is not changed):

$$x'_p = x_p \cos\omega' + y_p \sin\omega'$$

$$y'_p = -x_p \sin\omega' + y_p \cos\omega'$$

$$x'_c = x_c \cos w' + y_c \sin w'$$

$$y'_c = 0$$

The distance h between the center of the detector face to the tracer location and the radius ρ, indicating the distance of the tracer from the detector axis, are given by:

$$h = \left|x'_c - x'_p\right|, \qquad \rho = \sqrt{\left(y'_c - y'_p\right)^2 + \left(z'_c - z'_p\right)^2}$$

The equation of the circle for the reactor perimeter in the horizontal cross section remains the same, i.e.,

$$x^2 + y^2 = R_i^2 \ (\text{or } R_0^2)$$

where, R_i and R_o are the reactor inner and outer radii, respectively.

2) Rotation in the y'-z' plane by an angle ω" to for the projection of the 3-D line (x'_p, y'_p, z'_p) to (x'_c, y'_c, z'_c) on the y'-z' plane parallel to the new z" axis:

$$\omega'' = \tan^{-1}\left(\frac{y'_c - y'_p}{z'_c - z'_p}\right) \qquad \text{if} \qquad z'_c \neq z'_p$$

$$\omega'' = \frac{\pi}{2} \qquad \text{if} \qquad z'_c = z'_p$$

The tracer particle (subscript p) and the detector (subscript c) positions in the new coordinate system are:

$$x''_p = x'_p$$

$$y''_p = -z'_p \sin\omega'' + y'_p \cos\omega''$$

$$z''_p = z'_p \cos\omega'' + y'_p \sin\omega''$$

$$x''_c = x'_c$$

$$y''_c = -z'_c \sin w'' + y'_c \cos w''$$

$$z''_c = z'_c \cos w'' + y'_c \sin w''$$

The equation of the circle for the reactor perimeter in the horizontal cross section in the new coordinate system becomes:

$$x^2 + \left(-z \sin w'' + y \cos w''\right)^2 = R_i^2 \ (\text{or } R_0^2)$$

The direction cosines (cos α", cos β", cos γ") of the γ-ray path from the tracer location to the entry point on the detector can now be related to the angles α and θ (from the detector point of view) by:

$$\cos\alpha'' = \cos\theta_1, \qquad \cos\beta'' = \sin\theta_1 \sin\alpha, \qquad \cos\gamma'' = \sin\theta_1 \cos\alpha$$

where, $\theta_1 = \theta$ if $z''_p \leq z''_c$, otherwise, $\theta_1 = \pi - \theta$.

After knowing the direction cosines of the path (particle to γ-ray entry point), the path equations can be written as:

$$x = x_p'' + t\cos\alpha''$$

$$y = y_p'' + t\cos\beta''$$

$$z = z_p'' + t\cos\gamma''$$

where, t is the parameter defining the line in a 3-D space.

These linear equations can be solved along with the reactor circle equation to obtain the intersection point of the γ-ray path with the reactor inner diameter, ID, and the reactor outer diameter, OD. Once these parametric equations are substituted into the circle equation, one gets a quadratic equation in t (parameter defining a line in 3-D) which has an analytical solution. Once t is known, the equations above, defining the 3-D line, are used to compute the intersection points with the reactor inner and outer walls. There are two intersection points for each circle equation. The one closer to the detector is the true solution, whereas the other is discarded. The distance traveled by a γ-ray inside the reactor media, d_r, and through the reactor wall, d_w, can then be determined by the particle position and intersection points, i.e.

$$d_r = \sqrt{\left(x_p'' - x_{id}''\right)^2 + \left(y_p'' - y_{id}''\right)^2 + \left(z_p'' - z_{id}''\right)^2}$$

$$d_w = \sqrt{\left(x_p'' - x_{od}''\right)^2 + \left(y_p'' - y_{od}''\right)^2 + \left(z_p'' - z_{od}''\right)^2} - d_r$$

where, (x_{id}, y_{id}, z_{id}) is the intersection point with the reactor inner wall, ID, and (x_{od}, y_{od}, z_{od}) is the intersection with the reactor outer wall, OD.

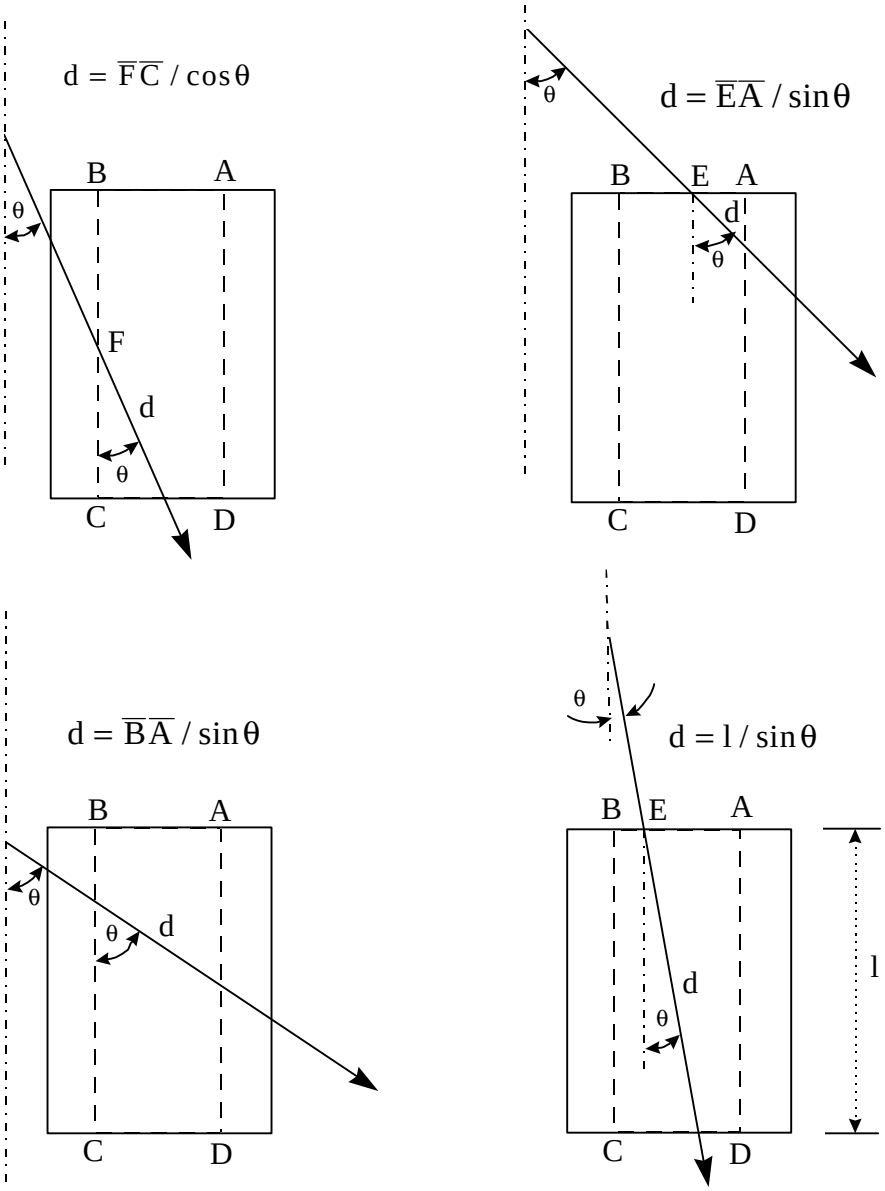

Figure 5.3: The Four Possible Cases of Travel of Photons Through the Detector

Having calculated the distances a photon travels through the reactor media and through the reactor wall, one has to determine next the location on the detector surface where the photon is going to enter the crystal. Subsequently, one needs to determine where the undisturbed γ-ray is going to exit the detector. Depending on h, α, ρ and θ, there could be four possible combinations of where a photon enters and where it exits the detector crystal (Figure 5.3). Through firm mathematical arguments (not presented here), one determines the effective distance, d, which a photon travels through the detector undisturbed, as well as the initial direction cosines and the first interaction site of the photon with the crystal (which is the already known position where the photon enters the crystal).

With the initial direction cosines and the site of the first interaction known, the locations of the subsequent interaction sites are obtained from

$$X_{N+1} = l' \cos\alpha + X_N , \qquad Y_{N+1} = l' \cos\beta + Y_N, \qquad Z_{N+1} = l' \cos\gamma + Z_N$$

In the above equations, $\cos\alpha$, $\cos\beta$ and $\cos\gamma$ are the direction cosines after the N^{th} interaction, l' is the photon path length between interaction sites, which is determined from another rectangularly distributed random number between 0 and 1, n''

$$n'' = \frac{\int_0^{l'} e^{-\mu x} dx}{\int_0^{d} e^{-\mu x} dx} \qquad \text{or} \qquad l' = \frac{-\ln\{1 - n''(1 - e^{-\mu d})\}}{\mu}$$

The energy of a photon is reduced in accordance with the Klein-Nishina differential scattering cross-section (not discussed here). The scattered angle θ is given by the Compton scattering law

$$\cos\theta = 1 + 0.511/E_0 - 0.511/E$$

where, E_0 is the initial photon energy before scattering, and E is the photon energy afterwards. The azimuthal angle of the scattered path relative to the incident path is found at random from 0 to 2π by using another rectangularly distributed random number n'''

$$\phi = 2\pi n'''$$

The new direction cosines after scattering are

$$\cos\alpha' = \cos\alpha \cos\theta + (\cos\alpha \cos\gamma \sin\theta \cos\phi - \cos\beta \sin\theta \sin\phi)/(1 - \cos^2\gamma)^{1/2}$$
$$\cos\beta' = \cos\beta \cos\theta + (\cos\beta \cos\gamma \sin\theta \cos\phi + \cos\alpha \sin\theta \sin\phi)/(1 - \cos^2\gamma)^{1/2}$$
$$\cos\gamma' = \cos\gamma \cos\theta - \sin\theta \cos\phi \, (1 - \cos^2\gamma)^{1/2}$$

However, when $(1 - \cos^2\gamma)$ approaches zero, the following degenerate form is used:

$$\cos\alpha' = \sin\theta \cos\phi$$
$$\cos\beta' = \sin\theta \sin\phi$$
$$\cos\gamma' = \cos\gamma \cos\phi$$

With the new direction cosines, and the coordinates of the new interaction site, the new distance a photon can travel from the interaction site to the wall of the detector along the scattering path is required. This is done in the same way as while calculating the distance d, which a photon travels through the detector undisturbed.

This process of computing new direction cosines, and new interaction sites is continued until either the photon energy, E drops to 0.01 MeV, or the ratio of scattering to total cross-section drops to 10^{-10}. This process is repeated for all the Gaussian points in both

the directions, and the integrals evaluated for the total and photo-peak efficiencies. Table 5.1 lists the differences in our formulation from that of Beam *et al.* (1978).

Table 5.1: Comparison of Beam's Formulation to the Formulation Used in This Work

Method of Beam *et al* (1978)	**Method used in this work**
$\Omega = \frac{4\pi}{N}\sum_{i=1}^{N} w(\alpha_i,\theta_i)$	$\Omega = \pi\sum_{i=1}^{n}\sum_{j=1}^{n} w_g(i)w_g(j)w(\alpha_i,\theta_j)$
$T_\varepsilon = \frac{1}{N}\sum_{i=1}^{N} w(\alpha_i,\theta_i)f_a(\alpha_i,\theta_i)f_d(\alpha_i,\theta_i)$	$T_\varepsilon = \frac{1}{4}\sum_{i=1}^{n}\sum_{j=1}^{n} w_g(i)w_g(j)w(\alpha_i,\theta_j)f_a(\alpha_i,\theta_j)f_d(\alpha_i,\theta_j)$
$P_\varepsilon = \frac{1}{N}\sum_{i=1}^{N} w(\alpha_i,\theta_i)f_a(\alpha_i,\theta_i)f_p(\alpha_i,\theta_i)$	$P_\varepsilon = \frac{1}{4}\sum_{i=1}^{n}\sum_{j=1}^{n} w_g(i)w_g(j)w(\alpha_i,\theta_j)f_a(\alpha_i,\theta_j)f_p(\alpha_i,\theta_j)$
$\alpha_i,\theta_i \equiv$ determined by the tracer and the point where the gamma-ray enters the	$w_g(i) \equiv$ weight corresponding to the Gaussian $x_g(i)$, which corresponds.
$N \equiv$ number of randomly gamma-ray histories, ~ 10000 for accurate	$w_g(j) \equiv$ weight corresponding to the Gaussian $x_g(j)$, which corresponds .
	$n \equiv$ number of Gaussian points in each ~ 30 are enough to give accurate values the multi-dimensional

5.3.3. Computation of Simulated Counts

Once the detector photo-peak efficiency has been simulated, the radioactive counts registered by each detector are evaluated. The number of γ-ray peaks received by NaI detector obeys the nonparalyzable model, and the detector count is mathematically expressed as:

$$C = \frac{T\nu^* GRP_\varepsilon}{1+\tau\nu^* GRP_\varepsilon}$$

$T \equiv$ sampling time.

$\nu^* \equiv$ number of γ-rays emitted per disintegration (2 for $Sc^{46)}$.

$G \equiv$ detector gain factor.

$R \equiv$ source strength (activity), disintegrations/second.

$P_\varepsilon \equiv$ photo-peak efficiency or full-energy peak efficiency.

$\tau \equiv$ dead time of the detector.